

A Portable Diagnostic Device for Cardiac Magnetic Field Mapping

J. W. Mooney, S. Ghasemi-Roudsari, E. Reade Banham, C. Symonds, N. Pawlowski, and B. T. H. Varcoe

School of Physics and Astronomy, University of Leeds, Leeds LS2 9JT, UK

June 2016

Abstract. In this paper we present a portable magnetocardiography device. The focus of this development was delivering a rapid assessment of chest pain in an emergency department. The aim was therefore to produce an inexpensive device that could be rapidly deployed in a noisy unshielded ward environment. We found that induction coil magnetometers with a coil design optimized for magnetic field mapping possess sufficient sensitivity ($104fT/\sqrt{Hz}$ noise floor at 10Hz) and response ($813fT/\mu V$ at 10Hz) for cycle averaged magnetocardiography and are able to measure depolarisation signals in an unshielded environment. We were unable to observe repolarisation signals to a reasonable fidelity. We present the design of the induction coil sensor array and signal processing routine along with data demonstrating performance in a hospital environment.

PACS numbers: 06.30.Ka, 41.20, 87.19, 87.57.-s

1. Introduction

Chest pain is responsible for one of the highest rates of emergency hospital visits in industrialized countries [1] and accounts for a large proportion of hospital admissions. Statistics show that around 75% of patients who present at the Emergency Department with chest pain do not have a cardiac related condition [2–5], yet they still need to go through a full diagnostic pathway which can take more than 10 hours [2]. This leads to several thousand people occupying bed spaces placing an additional burden on health care systems. A diagnostic that is capable of rapidly stratifying the cases and removing those patients who don't need an overnight stay is therefore valuable in both triage and cost saving [2].

Magnetocardiography (MCG) involves capturing Magnetic Field Maps (MFM's) of current distributions resulting from cardiac action potentials [6–14]. It has been shown that MCG gives significant improvements in diagnostic capability over an ECG [15–26]. Significantly, in this respect, it has been demonstrated that MCG is capable of reliable detection of Non-ST-Elevated Myocardial Infarction (NSTEMI) [15, 22], which are by definition difficult to detect using ECG. For this reason all ECG negative chest

pain patients are treated as having an NSTEMI until other diagnostic results can be obtained [3]. Hence, the short time to produce a MCG (typically <10 minute measurement) dramatically reduces the time for diagnosis and removes otherwise healthy patients earlier in the process and is therefore a tool with obvious clinical benefits.

The principle focus of the current research was the creation of a portable MCG device that would be capable of providing a rapid assessment of acute coronary syndrome (ACS) in an Emergency Department. To meet this goal, the device requirements are sensitivity to a magnetic window of between 0.1pT and 300pT, in the frequency range of around 1–40 Hz [27] and a spatial resolution sufficient to detect anomalies with a spacing of 10–15cm (for a sensor operated 10cm from the chest wall) [28].

Cardiac MFM devices typically use an array of sensitive magnetometers detectors to collect the magnetic field of the heart by simultaneously sampling at many positions across the chest. Sensors include liquid helium cooled SQUID detectors, which have been used in commercially available devices for over 40 years [29], and atomic physics detectors and giant magnetoresistance detectors have also been developed [27, 30, 31].

These devices are not always suitable for an Emergency Department as the associated apparatus is bulky, they often require liquid helium, specialist training to use, they are fixed in place and typically require an electromagnetically shielded room. In contrast, induction coil magnetometers have been used several times for cardiac magnetic field detection by several authors. They meet the demands of signal sensitivity [32–37], they are inexpensive, do not require cooling and can be run from batteries. However earlier efforts required noisy high gain amplifiers, large and heavy coils which are unsuitable for magnetic field mapping and fixed electronically implemented gradiometer arrangements. Here we present a more compact coil design which when combined with modern analog-to-digital converters (ADC's) and digital signal processing (DSP) produces a device capable of detecting the cardiac magnetic field with an array of 19 sensors.

We first present the design of the sensors, array and DSP routine. Then we show that this design has the capability of resolving the field of the heart within both shielded and unshielded environments.

2. Apparatus

2.1. Coil Design

The most important aspect of this device is the construction of the sensor elements to achieve both the sensitivity and required spatial resolution. An induction coil magnetometer will have an output voltage determined by

$$V = AN \frac{dB(t)}{dt} = ANB2\pi f \quad (1)$$

where N is the number of windings, A is the effective cross sectional area of the coil, $B(t)$ is the time varying magnetic field, with a magnitude B , and f is the frequency

of oscillation of the field. The smallest field, S , that can be detected given thermal Johnson noise resulting from the winding resistance is given by: detected given thermal Johnson noise resulting from the winding resistance is given by:

$$S = \frac{\sqrt{4k_B T R_a}}{2\pi f N A} \quad (2)$$

where k_B is Boltzmann's constant, T is the temperature, R_a is the antenna wire resistance given by:

$$R_a = N 2\pi^2 a^2 \rho r_{coil} \quad (3)$$

where a is the radius and ρ is the resistivity of the wire used in the windings on a circular coil of average winding radius r_{coil} . Equations 1, 2 can be used to find the coil structure with lowest noise level given the design constraints.

If the coil parameters are the length L , the coil outer diameter, D , and the coil inner diameter, D_i , the dimensions that give the lowest noise level have the ratio $D_i : D = 0.425 : 1$. In addition to this we primarily want to measure the component of the magnetic field aligned to the axis of the coil. Zilstra [38] notes that the optimum coil structure to measure the axial component of the magnetic field is achieved when $L/D = 0.69$ for the above ratio D_i/D . The coil diameter itself is determined according to the desired device resolution, leaving the radius of the wire only remaining free parameter in the coil design.

The output voltage of the coil is determined by N . As all other parameters are now fixed, voltage is determined exclusively by the wire radius a . A thinner wire increases the voltage output at the expense of increased coil resistance and subsequently increased noise, leading to a fixed signal to noise ratio irrespective of wire diameter.

Table 1 presents outputs from a simulation of the coil design presented here (MFM Coil) compared to the Brooks coil of the same outside dimension and wire diameter, $a = 0.23mm$. A Brooks coil is a special case in which the ratio of the dimensions are chosen to optimise inductance for which the ratio of the dimensions are $D : D_i : L = 4 : 2 : 1$. The current MFM Coil design has a higher voltage and a lower noise equivalent field at the target frequency of 30Hz than the Brooks coil. The noise equivalent field is the smallest field strength that could be measured above Johnson noise of the detector. The gains are a factor of 1.6 in signal to noise and a factor of about 2.9 in output voltage.

The increased signal size plays a role in the subsequent electronics especially when thermal and Johnson noise in the electronics is similar in size to the cardiac signal. Overall both effects improve data collection times by a factor of 20. This is important because, while the gains are modest, the overall impact on the design is a significant reduction (more than an order of magnitude) in the data collection time when cycle averaging is used.

Table 1. Table comparing the classic Brooks coil design with the MFM coil design presented in this paper.

Coil	D	D_i	L	V_{out} at 1pT (40Hz)	Noise Equivalent Field
MFM	12cm	5.1cm	8.28cm	616nV	57fT
Brooks	12cm	6cm	3cm	211nV	96fT
MFM	8.5cm	3.6cm	5.87cm	155nV	136fT
Brooks	8.5cm	4.25cm	2.125cm	53nV	227fT
MFM	4.25cm	1.8cm	2.9cm	9.5nV	773fT
Brooks	4.25cm	2.125cm	1.0625cm	3.3nV	1.3pT

2.2. Mapping Array Construction

The commercial analog to digital converter (ADC) we used has 16 channels. One channel was reserved for the ECG trigger, leaving 15 cardiac magnetometer channels. MFM Coils with a diameter of 7cm were chosen to cover the measurement area of $\sim 25 \times 25\text{cm}$ in a hexagonal array, arranged in order to detect the principle components of the hearts magnetic dipole field.

To evaluate the mapping fidelity of this arrangement a COMSOL model of the array was created. The interaction of the soft iron cores with a static magnetic dipole field comparable in size to the cardiac dipole was simulated. Measurements of the flux at the coil centers were taken as readings equivalent to sensor output. These outputs were spatially interpolated using the same technique as used with actual sensor signals to produce MFM. From the MFM the field map angle (FMA) was measured from the vector between the dipole maxima. Figure 2 shows the actual and measured MFM's at a fixed angle. The simulated cardiac dipole was rotated in small increments. At each increment the difference between the actual angle and the measured angle was calculated. The maximum difference observed was 15° , with a typical error of 8° . This uncertainty can be reduced by taking the vector between pole centroids, this spatially averaged measurement of the dipole vector has a considerably lower uncertainty of $< 1^\circ$.

To collect cardiac magnetic fields we designed a mount to hold up to 19 coils with a hexagonal close packed layout of sensor locations, see Figure 4. The layout, the approximate location against the body and a system level diagram for data acquisition are shown in figure 3. Since movement of the coils within the Earth's field will induce a current in the coils, they must be stiffly coupled so that acoustically induced signals become common mode and therefore removable by gradiometry. To this end, the mount was manufactured from a single piece of Acetal engineering plastic and the coils were securely potted in place. It was supported above the suppine participant by a four legged aluminium frame coupled to the floor. The large mass provided inertial dampening.

2.3. Data Acquisition and DSP

To extract signal from the coils with minimum interference a low noise pre-amplifier ($3.5\text{nV}/\sqrt{\text{Hz}}$ at 10Hz) with a gain of $1000\times$ was placed immediately above each MFM

Coil, see Figure 5 for details. The signal was then digitized using a National Instruments 16-channel 2kS/s 24bit AC-coupled ADC with a rail-rail voltage of 316mV (37nV sensitivity). Cycle averaging, filtering and gradiometry were performed in digital post processing [39].

Cycle averaging used the ECG R-wave rising edge as a fiducial. The magnetometer signals were sliced in an interval of $\pm 500ms$ about the fiducial, these intervals were then averaged. A moving average filter was applied by convolution of the signal with a 20ms wide top hat distribution [40].

In the normal mode of operation of a magnetic gradiometer it is considered necessary to have extensive shielding or closely matched gradiometer coils. But matching wire wound induction coils to sufficient accuracy is effectively impossible. However, in an array of coils differences in coil sensitivity are reduced by taking the average, and since the spatial average over a dipole crosssection is zero, the cardiac signal is not present in this background. Hence, this background is a bucket detector. Subtracting the bucket detector signal from a sensor signal produces a gradiometric signal.

Induction coils measure the time derivative of the magnetic field and not the static field. It is not possible to accurately construct the static field components by integrating their signals since the constant of integration is unknown. Attempting to numerically integrate yeilds signals with large baseline wander. This makes induction coil magnetometers not ideal for low frequency field measurement, though their performance can be improved with a fluxgate arrangement [41] or mechanical dithering of the sensors [42]. The derivative signals do not contain reliable absolute amplitude information, but they contain the same relative amplitude information and therefore the normalised spatial measurement is unaffected. Therefore the majority of the diagnostic information is preserved.

3. Results And Discussion

3.1. Sensor Response and Sensitivity

The sensor response was measured by placing one in the center of a helmholtz coil pair, applying a calibrated sinusoidal field and measuring the sensor output amplitude, as shown in Figure 6. The applied magnetic field amplitude was measured using a calibrated fluxgate magnetometer. The response is dependent on the field frequency and for this coil, it is linear between 1Hz and 1KHz. The measured response was $290fT/\mu V$ at 30Hz and $813fT/\mu V$ at 10Hz.

The sensitivity is determined by the inherent sensor noise. To measure the inherent noise the sensor was placed in a shielded room and 10 minutes of signal were recorded. Computing a FFT on this timeseries gives the amplitude spectral density of the sensor, see Figure 7. This voltage amplitude spectra was converted into magnetic field amplitude by factoring in the coils frequency response. The resulting noise floor was $104fT/\sqrt{Hz}$ at 10Hz and $36fT/\sqrt{Hz}$ at 30Hz.

3.2. First MCG Measurements

Now we show that these coils can detect the magnetic field with sufficient sensitivity and sufficiently low inherent noise. An MCG was taken in a shielded environment, where the environmental noise was low enough to observe dominant sensor noise. Figure 8d shows a raw MCG sensor signal taken from one of us in a shielded room which had an attenuation of 40dB at 1Hz and a maximum attenuation of 104dB at 30Hz. Approximately 10 minutes of data were recorded containing 485 cardiac cycles over 12 coils. The noise amplitude was approximately 0.6mV RMS ($< 73pT$).

The synchronously recorded 3 lead ECG shown in Figure 8b was thresholded to find the R-wave rising edge, this was used as a fiducial for cycle averaging, which reduced the noise amplitude by a factor of 35 (to $< 2.1pT$). Then the gradient was calculated by subtracting the synthetic bucket detector. However, this did not reduce the noise amplitude since it was composed of Johnson thermal noise which is uncorrelated across the array. Finally a 20ms wide moving average filter was applied to notch out the remaining 50Hz noise and smooth the remaining thermal noise.

The resulting signal has no significant noise ($< 150fT$) and corresponds with the anti-derivative of previously observed MCG signals [43,44]. It has a maximum amplitude during cardiac depolarisation of 0.05mV ($30pT$).

To analyse the device performance in an unshielded environment an MCG was recorded at Leeds General Infirmary, the results are shown alongside the shielded data in Figure 8. Similarly 10 minutes of data were recorded, yielding 482 cardiac cycles. The noise amplitude is much larger compared to the shielded room signals at 80mV ($\sim 20nT$), and highly correlated across the array. Cycle averaging reduces this by a factor of 12. Application of synthetic gradiometry provides $10\times$ rejection. The same 20ms wide moving average filter is highly effective at removing the remaining 50Hz noise and its harmonics leading to $500\times$ suppression. The resulting signal is the same amplitude as acquired in the shielded room, however there is a large coloured noise content.

This coloured noise could be removed by the application of more advanced DSP techniques such as wavelet denoising [45], reference data based non-linear denoising as an alternative improvement to gradiometry [46], and EEMD for baseline wander removal [47]. A second layer of coils ontop could provide an improvement to gradiometer performance as the second coils would be coaxial with the first but receive reduced cardiac magnetic flux [48].

The sensitivity to low frequency could be increased by lock-in to a global excitation field provided by a fluxgate or mechanical dithering arrangement [41, 42, 49–51].

MFM's represent the magnetic field at a chosen instant in the cardiac cycle. They are created by spatially interpolating the sensor amplitudes from a common time sample. Figure 9 compares the shielded and unshielded MFM's at -15ms, during the magnetic R wave peak activity.

The dipole angle is consistent between the two MFM's. The dipole position is

translated between the MFM's since the array was only subjectively aligned in the coronal plane relative to the Xiphoid process. Also the angle between the coronal and transversal planes was not precisely controlled, since each bed had a different distribution of padding material. Ideally the MFM would be precisely referenced to the individuals cardiac geometry. This would be invaluable for solving the inverse problem; estimating the structure of the underlying current distribution corresponding to the observed MFM.

The observed dipole angle and size are in good agreement with past MCG observations of healthy normals [22]. We therefore anticipate that the signal has similar diagnostic value.

4. Conclusion

We have presented a new design for a device to perform magnetic field mapping and demonstrated that the device collects useful magnetocardiography data in shielded and unshielded environments.

The shielded measurements prove that the coil sensor system has sufficiently low inherent noise for cycle averaged MCG and sufficient spatial resolution for field map angle measurement.

However, operation of the device within an unshielded environment imposes coloured noise on the signal of an amplitude comparable to the repolarisation signals (ECG T wave). This potentially limits the diagnostic capability of our device within unshielded environments. Though the depolarisation signals (QRS) are reliably observable above this noise. This result may be improved by the application of recent developments in denoising algorithms [45–47].

Further clinical testing will be required to determine if it is capable of detecting recent onset of NSTEMI in patients with the same accuracy as previous devices. A future device may want to use more sensors to increase the measurement area and may also consider smaller coils to achieve a higher resolution. The addition of a second layer of coils would provide a vertical baseline for synthetic gradiometry which may improve environmental noise suppression [48]. The low frequency performance could be improved to reach DC by lock-in to a global excitation field [41, 42, 49–51].

5. Acknowledgments

Permission to use human subjects in the collection of data was granted by the University of Leeds ethics committee (ref. no. MEEC 12–034). This research would not have been possible without the assistance of L. Falk, R. Byrom, M. Williamson, D. Brette, Prof. M Kearney and S. Smye at LGI and M. Everitt, S. Brown, L. Burgin, F. Ridgeon, B. Gibbs, P. Thornton, D. Grimmond, M. Moran, and S. Mann at the University of Leeds. We thank Prof. G. Green at York Neuroimaging for access to the shielded room. We acknowledge funding from the NHS National Innovation Center, the IKC for Medical Devices, the BHRC, HEIF, IPGroup, Quantum Imaging Limited and the University of

Leeds. CS thanks Wellcome Trust and Nuffield for summer project support.

References

- [1] Miquel Sanchez, Beatriz Lopez, Ernest Bragulat, Elisenda Gomez-Angelats, Sonia Jimenez, Mar Ortega, Blanca Coll-Vinent, Josep R. Alonso, Carme Queralt, and Oscar Miro. Triage flowchart to rule out acute coronary syndrome. *The American Journal of Emergency Medicine*, 25(8):865–872, 2007.
- [2] A. J. Six, B. E. Backus, A. Kingma, and S. I. Kaandorp. Consumption of diagnostic procedures and other cardiology care in chest pain patients after presentation at the emergency department. *Netherlands Heart Journal*, 20(12):499–504, 2012.
- [3] B. E. Backus, A. J. Six, J. C. Kelder, M. A. R. Bosschaert, E. G. Mast, A. Mosterd, R. F. Veldkamp, A. J. Wardeh, R. Tio, R. Braam, S. H. J. Monnick, R. van Tooren, T. P. Mast, F. van den Akker, M. J. M. Cramer, J. M. Poldervaart, A. W. Hoes, and P. A. Doevendans. A prospective validation of the heart score for chest pain patients at the emergency department. *International Journal of Cardiology*, 168(3):2153–2158, 2013.
- [4] B.E. Backus, A.J. Six, J.H. Kelder, W.B. Gibler, F.L. Moll, and P.A. Doevendans. Risk scores for patients with chest pain: Evaluation in the emergency department. *Current Cardiology Reviews*, 7:2–8, 2011.
- [5] M. Rohacek, A. Bertolotti, N. Grutzmuller, U. Simmen, H. Marty, H. Zimmermann, A. Exadaktylos, and A. Spyridon. The challenge of triaging chest pain patients: the bernese university hospital experience. *Emergency Medicine International*, 2012(2090-2859 (Electronic)), 2012.
- [6] Hannu J. Eskola, J. A. V. Malmivuo, Juha J. O. Nousiainen, and Jukka O. Lekkala. Corrected unipositional lead system for vector magnetocardiography. *Biomedical Engineering, IEEE Transactions on*, BME-34(2):81–90, 1987.
- [7] Petri Korhonen, Juha Mointonen, Markku Mkinrvi, Toivo Katila, Markku S. Nieminen, and Lauri Toivonen. Late fields of the magnetocardiographic qrs complex as indicators of propensity to sustained ventricular tachycardia after myocardial infarction. *Journal of Cardiovascular Electrophysiology*, 11(4):413–420, 2000.
- [8] Petri Korhonen, Ilkka Tierala, Kim Simelius, Heikki Vninen, Markku Mkiirvi, Jukka Nenonen, Toivo Katila, and Lauri Toivonen. Late qrs activity in signal-averaged magnetocardiography, body surface potential mapping, and orthogonal ecg in postinfarction ventricular tachycardia patients. *Annals of Noninvasive Electrocardiology*, 7(4):389–398, 2002.
- [9] J. Malmivuo and R. Plonsey. *Bioelectromagnetism - Principles and Applications of Bioelectric and Biomagnetic Fields*. Oxford University Press, New York, 1995.
- [10] R. McFee and G. M. Baule. Research in electrocardiography and magnetocardiography. *Proceedings of the IEEE*, 60(3):290–321, 1972.
- [11] Werner Moshage, Stephan Achenbach, Konrad Gahl, and Kurt Bachmann. Evaluation of the non-invasive localization accuracy of cardiac arrhythmias attainable by multichannel magnetocardiography (mcg). *The International Journal of Cardiac Imaging*, 12(1):47–59, 1996.
- [12] Ceon Ramon, P. Czapski, J. Haueisen, Lee L. Huntsman, H. Nowak, G. H. Bardy, U. Leder, Kim Yongmin, and J. A. Nelson. Mcg simulations with a realistic heart-torso model. *Biomedical Engineering, IEEE Transactions on*, 45(11):1323–1331, 1998.
- [13] M. Saarinen, P. J. Karp, T. E. Katila, and P. Siltanen. The magnetocardiogram in cardiac disorders. *Cardiovascular Research*, 8(6):820–834, 1974.
- [14] F. E. Smith, P. Langley, U. Steinhoff, L. Trahms, J. P. Bourke, and A. Murray. Relation between spatial properties of repolarisation interval and t-wave amplitude using magnetocardiography. In *Computers in Cardiology 2001*, pages 629–632, 2001.
- [15] Rajender Agarwal, Abhimanyu Saini, Tareq Alyousef, and Craig A. Umscheid. Magnetocardi-

- graphy for the diagnosis of coronary artery disease: A systematic review and meta-analysis. *Annals of Noninvasive Electrocardiology*, 17(4):291–298, 2012.
- [16] R. Fenici, D. Brisinda, A. Venuti, and A. R. Sorbo. Thirty years of clinical magnetocardiography at the catholic university of rome: Diagnostic value and new perspectives for the treatment of cardiac arrhythmias. *International Journal of Cardiology*, 168(0), 2013.
- [17] Andrej Gapelyuk, Niels Wessel, Robert Fischer, Udo Zacharzowsky, Lydia Koch, Daniela Selbig, Henry Schtt, Bianca Sawitzki, Friedrich C. Luft, Rainer Dietz, and Alexander Schirdewan. Detection of patients with coronary artery disease using cardiac magnetic field mapping at rest. *Journal of Electrocardiology*, 40(5):401–407, 2007.
- [18] Birgit Hailer, Ilja Chaikovsky, Sabine Auth-Eisernitz, Harald Schaffer, and Peter Van Leeuwen. The value of magnetocardiography in patients with and without relevant stenoses of the coronary arteries using an unshielded system. *Pacing and Clinical Electrophysiology*, 28(1):8–16, 2005.
- [19] Petri Korhonen, Terhi Husa, Ilkka Tierala, Heikki Vaananen, Markku Makijarvi, Toivo Katila, and Lauri Toivonen. Increased intra-qrs fragmentation in magnetocardiography as a predictor of arrhythmic events and mortality in patients with cardiac dysfunction after myocardial infarction. *Journal of Cardiovascular Electrophysiology*, 17(4):396–401, 2006.
- [20] Boris Leithauser, Friedrich Jung, and Jai-Wun Park. Special article magnetocardiography in clinical cardiology. status quo and future applications. *Advances in Interventional Cardiology*, 3:215–222, 2011.
- [21] Hyun Kyoong Lim, Namsik Chung, Kiwoong Kim, Young-Guk Ko, Hyukchan Kwon, Yong-Ho Lee, Jin-Mok Kim, Boyoung Joung, Jin-Bae Kim, Kwon Kyu Yu, Jung-Rae Cho, In-Seon Kim, and Yong Ki Park. Can magnetocardiography detect patients with non-st-segment elevation myocardial infarction? *Annals of Medicine*, 39(8):617 – 627, 2007.
- [22] Hyun Kyoong Lim, Hyukchan Kwon, Namsik Chung, Young-Guk Ko, Jin-Mok Kim, In-Seon Kim, and Yong-Ki Park. Usefulness of magnetocardiogram to detect unstable angina pectoris and non-st elevation myocardial infarction. *The American Journal of Cardiology*, 103(4):448–454, 2009.
- [23] Jai-Wun Park, Peter M. Hill, Namsik Chung, Paul G. Hugenholtz, and Friedrich Jung. Magnetocardiography predicts coronary artery disease in patients with acute chest pain. *Annals of Noninvasive Electrocardiology*, 10(3):312–323, 2005.
- [24] FE Smith, P Langley, P van Leeuwen, B Hailer, L Trahms, and Steinhoff U. Comparison of magnetocardiography and electrocardiography: a study of automatic measurement of dispersion of ventricular repolarization. *Europace*, 8(10):887–893, 2006.
- [25] Martin Steinisch, Paul R. Torke, Jens Hauelsen, Birgit Hailer, Dietrich Granemeyer, Peter Van Leeuwen, and Silvia Comani. Early detection of coronary artery disease in patients studied with magnetocardiography: An automatic classification system based on signal entropy. *Computers in Biology and Medicine*, 43(2):144–153, 2013.
- [26] K. Tolstrup, B. E. Madsen, J. A. Ruiz, S. D. Greenwood, J. Camacho, R. J. Siegel, H. C. Gertzen, J. W. Park, and P. A. Smars. Non-invasive resting magnetocardiographic imaging for the rapid detection of ischemia in subjects presenting with chest pain. *Cardiology*, 106(4):270–276, 2006.
- [27] G. Bison, N. Castagna, A. Hofer, P. Knowles, J. L. Schenker, M. Kasprzak, H. Saudan, and A. Weis. A room temperature 19-channel magnetic field mapping device for cardiac signals. *Applied Physics Letters*, 95(17):173701–3, 2009.
- [28] Shou Guofa, Xia Ling, Jiang Mingfeng, and Dou Jianhong. Magnetocardiography simulation based on an electrodynamic heart model. *Magnetics, IEEE Transactions on*, 47(9):2224–2230, 2011.
- [29] Gerhard Stroink. *Forty Years of Magnetocardiology Biomag2010*, volume 28 of *IFMBE Proceedings*, pages 1–8. Springer Berlin Heidelberg, 2010.
- [30] M. Pannetier-Lecoecur, H. Polovy, N. Sergeeva-Chollet, G. Cannies, C. Fermon, and L. Parkkonen. Magnetocardiography with gmr-based sensors. *Journal of Physics: Conference Series*, 303(1):012054, 2011.

- [31] Vishal K. Shah and Ronald T. Wakai. A compact, high performance atomic magnetometer for biomedical applications. *Physics in Medicine and Biology*, 58(22):8153, 2013.
- [32] Gerhard M. Baule and Richard McFee. The magnetic heart vector. *American Heart Journal*, 79(2):223–236, 1970.
- [33] Gerhard Baule and Richard McFee. Detection of the magnetic field of the heart. *American Heart Journal*, 66(1):95–96, 1963.
- [34] D. Cohen and L. Chandler. Measurements and a simplified interpretation of magnetocardiograms from humans. *Circulation*, 39(3):395, 1969.
- [35] David Cohen. Magnetic fields around the torso: Production by electrical activity of the human heart. *Science*, 156(3775):652–654, 1967.
- [36] K. P. Estola and J. Malmivuo. Air-core induction-coil magnetometer design. *Journal of Physics E: Scientific Instruments*, 15(10):1110, 1982.
- [37] K. Tashiro. Proposal of coil structure for air-core induction magnetometer. In *Sensors, 2006. 5th IEEE Conference on*, pages 939–942, 2006.
- [38] H. Zijlstra. *Experimental methods in magnetism*. Elsevier North-Holland, 1967.
- [39] Fernando Prez and Brian E. Granger. Ipython: A system for interactive scientific computing,, 2007. DOI:10.1109/MCSE.2007.53.
- [40] Eric Jones, Travis Oliphant, Pearu Peterson, et al. SciPy: Open source scientific tools for Python, 2001–. [Online; accessed 2016-09-11].
- [41] Hikaru Karo and Ichiro Sasada. Magnetocardiogram measured by fundamental mode orthogonal fluxgate array. *Journal of Applied Physics*, 117(17):17B322, May 2015.
- [42] Ral Jurez-Aguirre, Sal M. Domnguez-Nicols, Elas Manjarrez, Jess A. Tapia, Eduard Figueras, Hctor Vzquez-Leal, Luz A. Aguilera-Corts, and Agustn L. Herrera-May. Digital Signal Processing by Virtual Instrumentation of a MEMS Magnetic Field Sensor for Biomedical Applications. *Sensors*, 13(11):15068–15084, November 2013.
- [43] Hans Koch, Ralf-Dieter Boussejot, Olaf Kosch, Cosima Jahnke, Ingo Paetsch, Eckart Fleck, and Bernhard Schnackenburg. A reference dataset for verifying numerical electrophysiological heart models. *BioMedical Engineering OnLine*, 10(1):1–15, 2011.
- [44] Akihiko Kandori, Kuniomi Ogata, Yasushi Watanabe, Noriko Takuma, Kimio Tanaka, Masahiro Murakami, Tsuyoshi Miyashita, Nobuo Sasaki, and Yuji Oka. Space-Time Database for Standardization of Adult Magnetocardiogram-Making Standard MCG Parameters. *Pacing and Clinical Electrophysiology*, 31(4):422–431, April 2008.
- [45] Yasuhiro Ishikawa, Hitoshi Horigome, Akihiko Kandori, Hiroshi Toda, and Zhong Zhang. Noise reduction by perfect-translation-invariant complex discrete wavelet transforms for fetal electrocardiography and magnetocardiography. *Int. J. Wavelets Multiresolut Inf. Process.*, 12(04):1460008, February 2014.
- [46] Karsten Sternickel, Arndt Effern, Klaus Lehnertz, Thomas Schreiber, and Peter David. Nonlinear noise reduction using reference data. *Physical Review E*, 63(3), February 2001.
- [47] Marcelo A. Colominas, GastN Schlotthauer, MarA E. Torres, and Patrick Flandrin. Noise-assisted emd methods in action. *Advances in Adaptive Data Analysis*, 04(04):1250025, 2012.
- [48] Chan Seok Kang, Kwon Kyu Yu, Kiwoong Kim, Hyukchan Kwon, Jin-Mok Kim, and Yong-Ho Lee. Simple simulation method for investigating the performance of a SQUID gradiometer corresponding to a baseline length. *Current Applied Physics*, 12(5):1319–1325, September 2012.
- [49] Shinsuke Nakayama, Kenta Sawamura, Kaneo Mohri, and Tsuyoshi Uchiyama. Pulse-Driven Magnetoimpedance Sensor Detection of Cardiac Magnetic Activity. *PLOS ONE*, 6(10):e25834, October 2011.
- [50] E. Paz, S. Serrano-Guisan, R. Ferreira, and P. P. Freitas. Room temperature direct detection of low frequency magnetic fields in the 100 pT/Hz0.5 range using large arrays of magnetic tunnel junctions. *Journal of Applied Physics*, 115(17):17E501, May 2014.
- [51] Robert Jahns, Henry Greve, Eric Woltermann, Eckhard Quandt, and Reinhard Knchel. Sensitivity enhancement of magnetoelectric sensors through frequency-conversion. *Sensors and Actuators*

A: Physical, 183:16–21, August 2012.

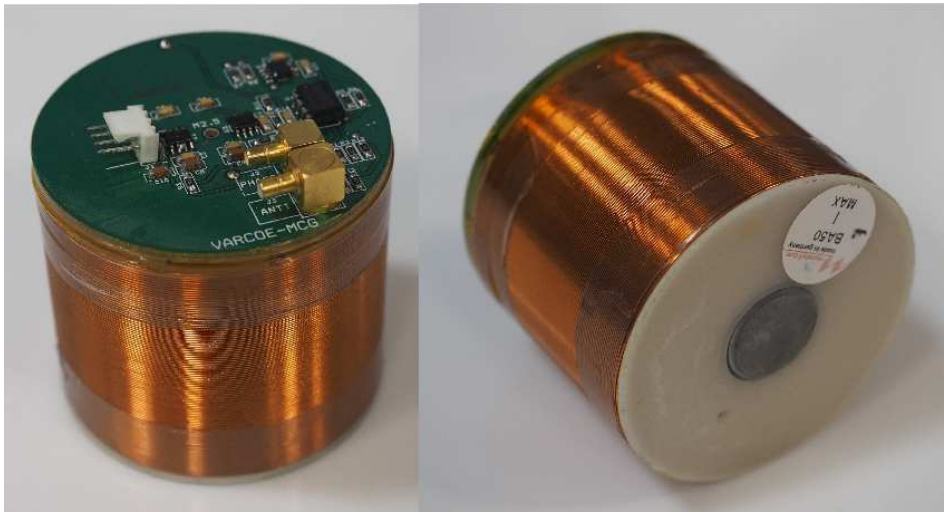


Figure 1. Photograph of the 7cm diameter coil sensors used. The 2cm diameter core is visible in the centre of the coil bobbin. The pre-amplifier circuit board is mounted to the coil to minimise the unshielded signal path. DC battery power is provided via the 4-way header. The amplified signals are output via an SMB connector into a coaxial cable.

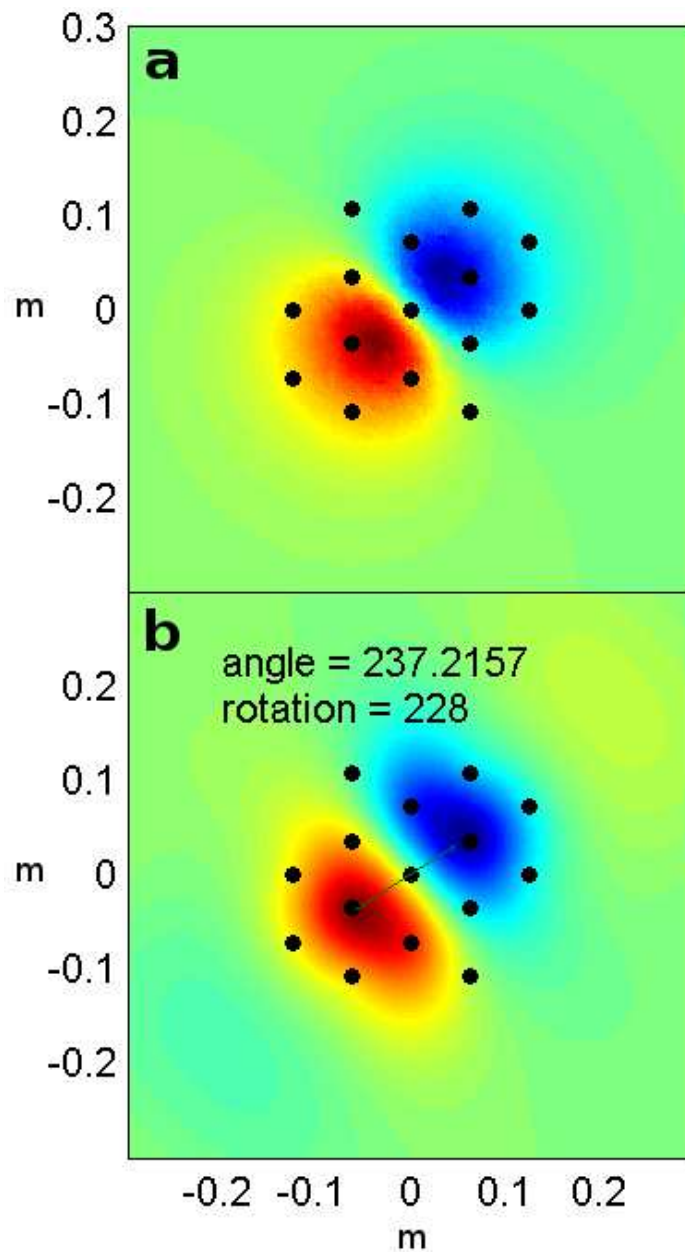


Figure 2. COMSOL model of the sensor array measuring an ideal cardiac dipole field. Figure a shows the cardiac dipole field, which is sampled at the center of the soft iron cores shown as black spots. Figure b shows the interpolated measurement of the field samples. The actual angle and the reconstructed rotation angle are closely matched indicating that an accurate reconstruction is possible with this sensor array.

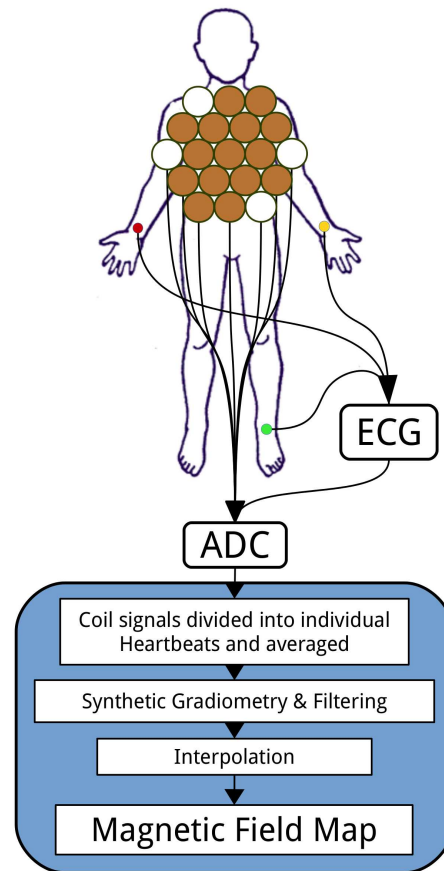


Figure 3. System level diagram; Individual pre-amplified sensor signals are acquired by the ADC, then processed within a computer to create a magnetocardiogram.

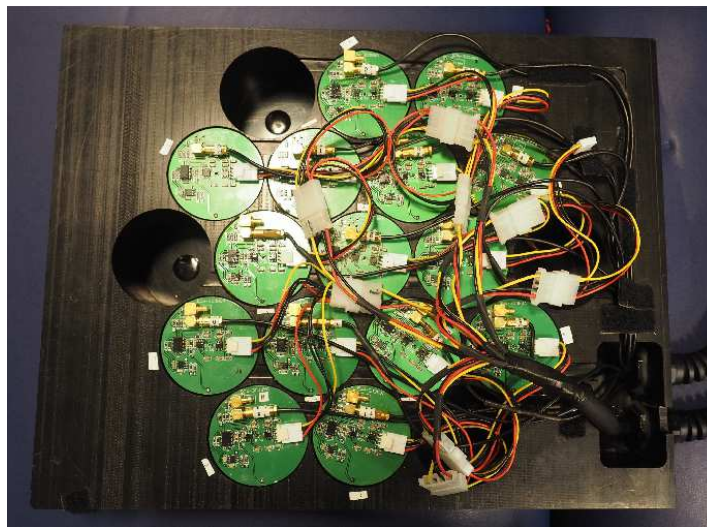


Figure 4. Photograph of the sensor array. The array was machined out of Acetyl engineering plastic, which stiffly couples the sensors together. This array was then bolted to an aluminium frame which supported it above a supine participant in order to capture MCG.

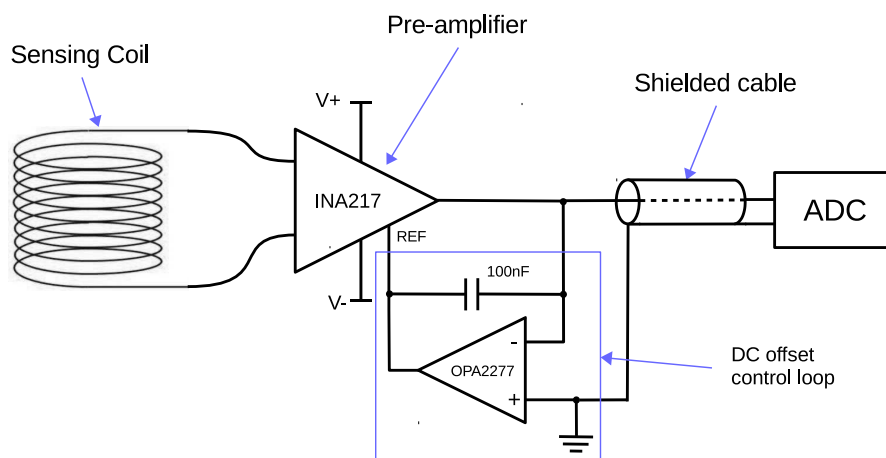


Figure 5. Schematic of a single sensor channel. The DC offset control loop is used to remove drift generated by the amplifier, it functions as a high pass filter with a cut-off of 1.6Hz. The amplifier power supply (V+, V-) is supplied by a pair of batteries with local fixed LDO voltage regulators.

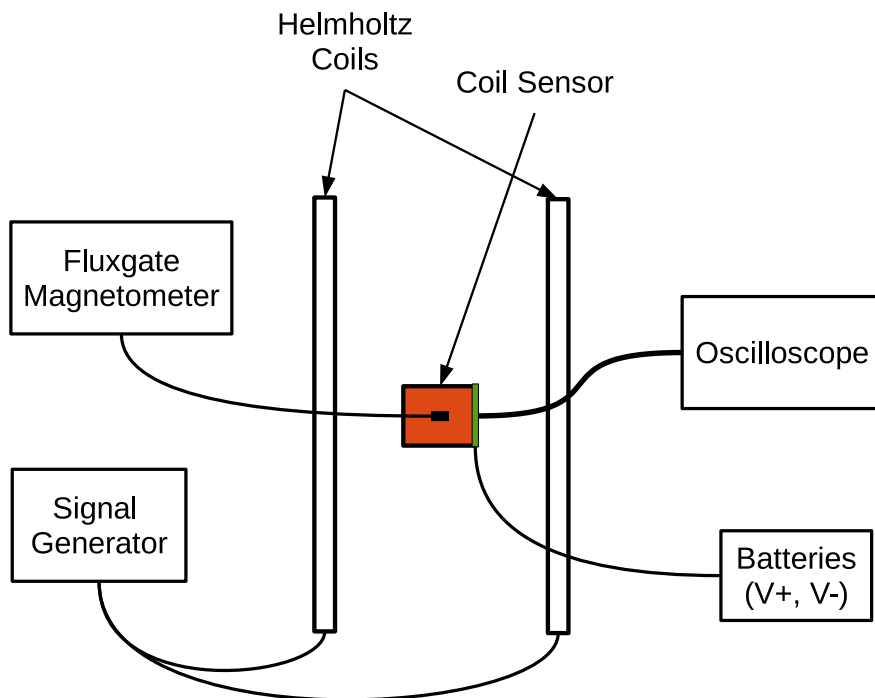


Figure 6. Experiment to measure sensor response. A sinusoidal field was created by the helmholtz coils being driven by the signal generator, the peak field amplitude was measured using a calibrated fluxgate magnetometer. The fluxgate probe was then replaced by a MFM coil sensor and the peak amplitude output by the sensor as recorded using the oscilloscope.

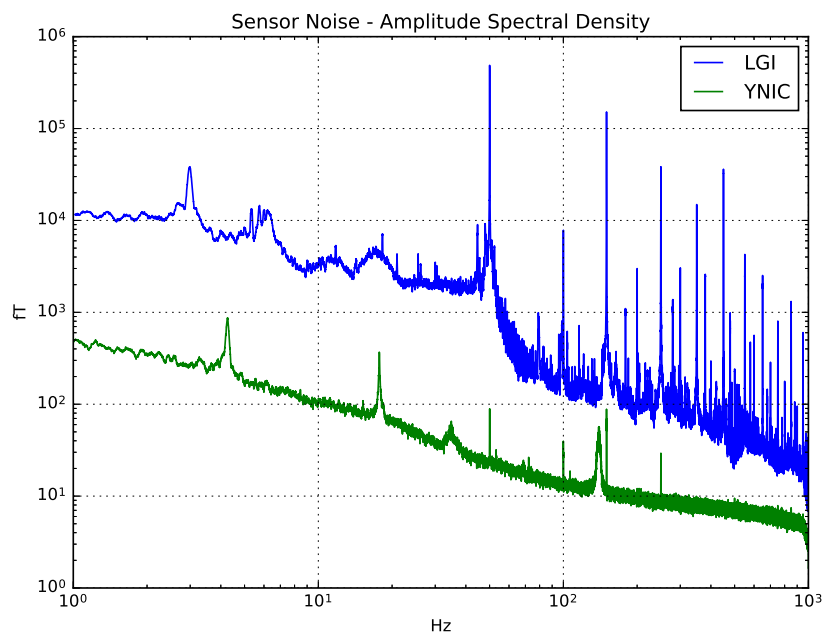


Figure 7. Amplitude spectral density of the sensor in shielded (YNIC) and unshielded (LGI) environments, computed by FFT. The sensor voltage spectral density was computed then the frequency dependent response was used to convert to units of magnetic field amplitude (fT).

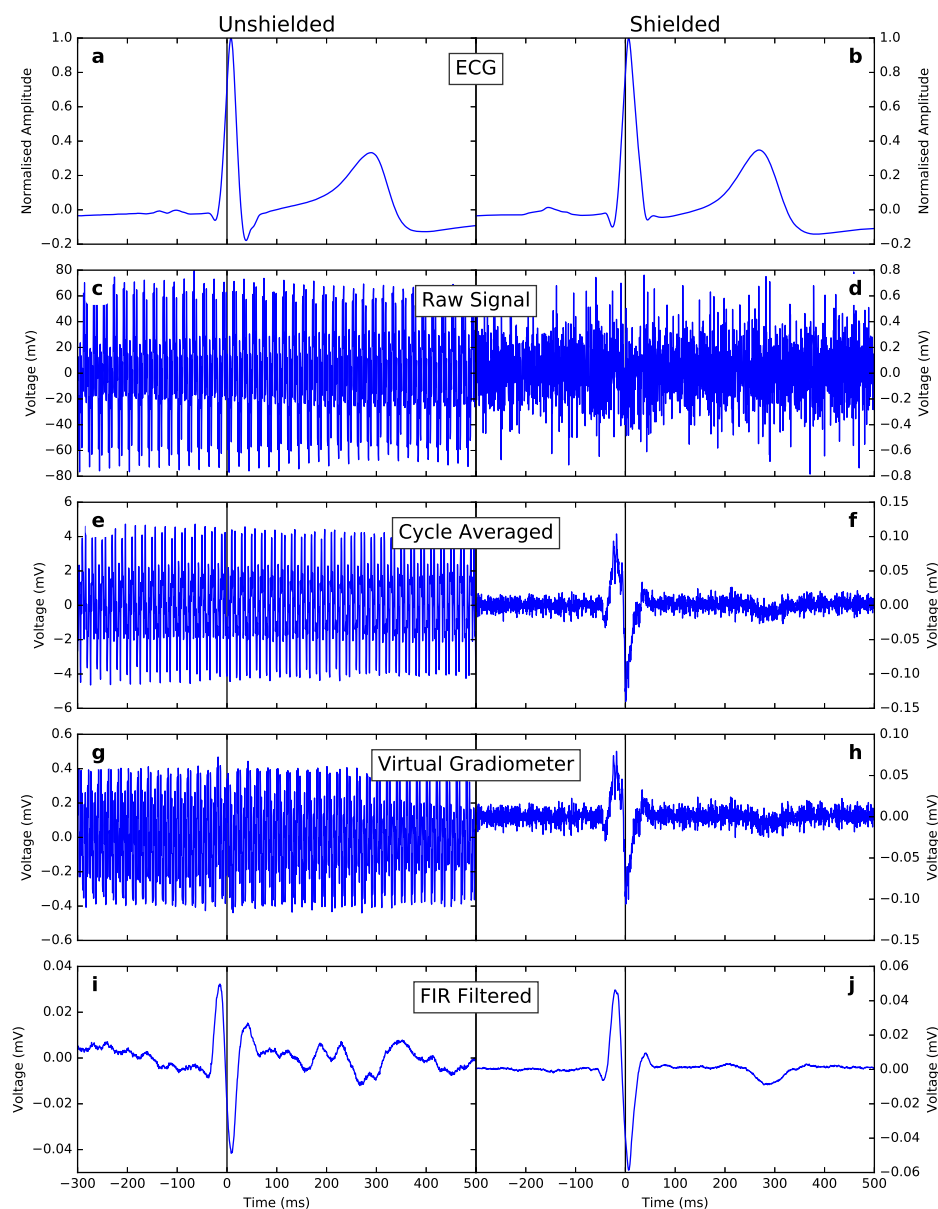


Figure 8. Comparison of two magnetometer signals from the same person taken with an identical device, with similarly positioned sensors but in different environments. The Shielded MCG was acquired in the York Neuroimaging center (YNIC). The Unshielded MCG was acquired at Leeds General Infirmary (LGI), 16 months later. The environmental noise is $100\times$ larger in LGI. Averaging reduces the noise amplitude by $20\times$. Gradiometry (subtracting the synthetic bucket detector signal) provides $10\times$ noise reduction at LGI but does not effect the noise amplitude at YNIC, in this case it reduces the signal amplitude as the dipole measurement was not symmetric. A final stage FIR filter notches out 50Hz, reducing LGI noise by $500\times$ and acting mostly as a smoothing filter in LGI with $20\times$ reduction. The final signal amplitudes differ by 40% which could be explained by a difference in sensor positioning or physiological differences. The unshielded signal has a similar level of white noise, but a much larger coloured noise component.

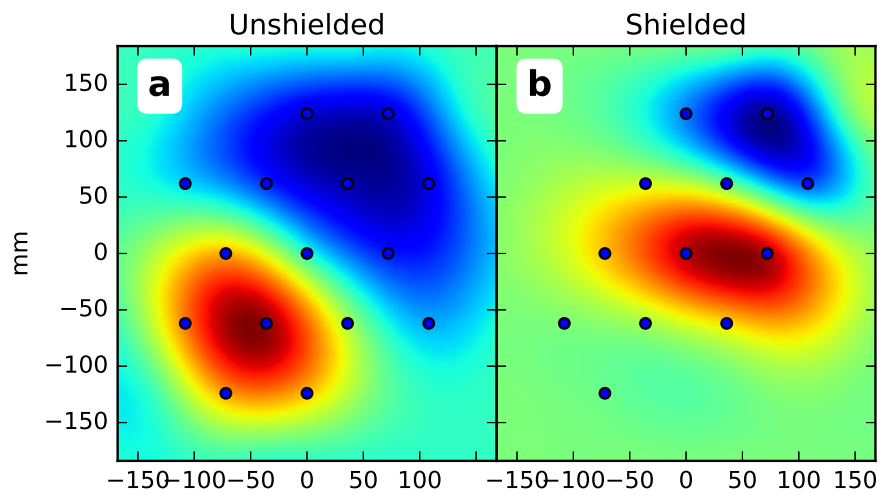


Figure 9. MFM's of the author, during the rising edge of the ECG r-wave. MFM on the left was taken in the YNIC shielded room. The MFM on the right was taken in an unshielded room at Leeds General Infirmary. The shielded measurement used 12 coils as the pre-amplifier wiring broke on three of the coils during transportation of the device to YNIC.